Appl Phys A
DOI 10.1007/s00339-008-4904-5

Applied Physics A
Materials Science & Processing

Modulating the diameter of carbon nanotubes in array form via floating catalyst chemical vapor deposition

Qiang Zhang · Jia-Qi Huang · Meng-Qiang Zhao · Wei-Zhong Qian · Fei Wei

Received: 26 May 2008 / Accepted: 8 September 2008

Abstract Based on the analysis of catalyst particle formation and carbon nanotube (CNT) array growth process in floating catalyst chemical vapor deposition (CVD), delicately controlled gaseous carbon sources and catalyst precursors were introduced into the reactor for the controllable growth of CNT array. The low feeding rate of ferrocene was realized through low-temperature sublimation. With less ferrocene introduced into the reactor, the collision among the *in situ* formed iron atoms decreased, which led to the formation of smaller catalyst particles. The mean diameter of the CNT array, grown at 800°C, decreased from 41 to 31 nm when the ferrocene-sublimed temperature reduced from 80 to 60°C. Furthermore, low growth temperature was adopted in synthesis, through the modulation of the CNT diameter, by controlling the sintering of catalyst particles and the collision frequency. When the growth temperature was 600°C, the as-grown CNTs in the array were with a mean diameter of 10.2 nm. If propylene was used as carbon source, the diameter can be modulated in similar trends. The diameter of CNT can be modulated by the parameter of the operation using the same substrate and catalyst precursor without other equipment or previous treatment. Those results provide the possibility for delicately controllable synthesis of CNT array via simple floating catalyst CVD.

PACS 81.07.-b · 81.07.De · 81.10.Bk · 81.16.-c · 61.46.-w

Q. Zhang (✉) · J.-Q. Huang · M.-Q. Zhao · W.-Z. Qian · F. Wei
Beijing Key Laboratory of Green Chemical Reaction Engineering and Technology, Department of Chemical Engineering, Tsinghua University, Beijing 100084, China
e-mail: zhang-qiang@mails.tsinghua.edu.cn

F. Wei (✉)
e-mail: weifei@flotu.org

1 Introduction

Since the first synthesis in 1996 [1], there has been increasing attention on controlling the growth of aligned carbon nanotube (CNT) arrays with desired morphologies, dimensions, and properties. These aligned CNTs in the arrays contain many attractive properties, such as identical tube length, uniform orientation, extra high purity, and easy spinning into macroscopic fibers. Therefore, the as-grown array can be directly used to construct field emission devices, anisotropic conductive materials, multifunctional membranes and super strong yarn. Even after the loss of the original alignment, longer and straighter multiwalled CNTs (MWCNTs) from the CNT arrays are found to be better in improving the electronic, mechanical, and thermal properties than randomly aggregated multiwalled or even single-walled CNT (SWCNT) in polymer reinforcements. In most cases, such as field emission display and composite application, small diameter CNTs in array form showed outstanding performance, which indicated that controllable fabrication of CNTs with small diameter was still a key problem [2].

Various synthesis methods have been developed. These include porosity-assisted chemical vapor deposition (CVD) [1], plasma-enhanced CVD [3], thermal CVD [4], alcohol-catalyzed CVD [5], and floating catalyst CVD [6–18]. CNTs grow on the catalyst particles from a carbon source in the CVD process. The growth mechanism has been well discussed in the literature, but the complete mechanism of growth is still not fully understood. The most accepted model for CNT growth is similar to the vapor–liquid–solid (VLS) mechanism [19, 20]. The catalytic decomposition of a carbon feedstock into carbon atoms and hydrogen was initiated on an active transition metal surface. This was followed by the diffusion of carbon into the metal particles, until the solution (metal–carbon) became saturated. When

supersaturated, the precipitation of graphite carbon occurred from the metal surface, which, under proper conditions, formed a cylinder (CNT). In the VLS model, the size of the active catalyst was a key factor in the diameter of the as-grown CNT. This was widely confirmed by many research groups [8–11, 21, 22]. Thus, for the diameter modulation, the catalyst formation and agglomeration became key factors.

In most of the thermal CVDs and plasma-enhanced CVDs, the catalyst particles are prepared by annealing metal film [3, 4, 23–25]. The film can be obtained by sputtering and electron evaporation using electroplating techniques. Thus, the size of the catalyst can be modulated by the thickness of the film and the annealing temperature [24, 25]. Additionally, some colloid particles can be used directly as catalysts for the CNT array growth, and the size of the colloid particle can be controlled by chemical routes [5]. Thin wall, even SWCNTs in array form can be obtained [26–28]. However, the above methods have limited productivity. The facilities for metal film formation are complex and expensive. The floating catalyst CVD method has the advantages of easy operation, cheap equipment, and lost cost, which attracted great interest from engineers to scale up the preparation of CNT array. In the floating catalyst CVD, the catalyst particles in situ formed first, and CNT arrays grew on the flat substrate. Singh et al. have reported the development of CNTs with a diameter distribution of 20–70 nm in array form synthesized using the ferrocene–toluene solution injection CVD method [13]. Tapaszto et al. have obtained 25–150 nm CNT array from a ferrocene–benzene precursor by spray pyrolysis [10]. Zhang et al. have reported fast CNT array growth with a diameter of 30–60 nm from a ferrocene–xylene mixture by using a floating catalyst CVD [9]. Xiang et al. have reported that the diameter of CNT array grown on spheres from cyclohexane was about 35 nm [29]. Compared with CNT array grown through thermal CVD, the CNT array grown from floating catalyst CVD is always larger than 20 nm. Until now, limited reports can be found for the diameter modulation of CNT in array form.

For the floating catalyst process, the catalyst particle was in situ formed through the decomposition of catalyst precursor and iron atom collision. Most studies used a solution to inject ferrocene into the reactor, which was convenient for controlling the feeding rate by pump [9–11]. However, the liquid-state carbon sources, like benzene, toluene, xylene, n-hexane, and cyclohexane, tended to simultaneously crack with the iron particle formation process [9–11, 15, 17, 30]. The carbon source decomposed quickly, and the CNTs in array form grew from the catalysts, which were distributed on the substrate. It was a complex, coupled process for the catalyst precursor and carbon source feeding together. In this article, ethylene, which was more stable gaseous carbon source than C_2H_2, benzene, toluene, and xylene, et al. was used as the carbon source, and ferrocene was used as a catalyst precursor. Instead of cofeeding with the carbon source, the catalyst precursor was sublimed in the present studies. Thus, the catalyst precursor can be controllably fed into the reactor by the evaporation temperature with a fixed flow rate of carrier gas. The related strategies for diameter modulation of CNT in the array form were discussed. Thin-wall CNT array with a diameter of 10 nm was obtained by lowering the feeding rate of the catalyst precursor and the growth temperature in the floating catalyst process.

2 Experimental details

The chemical reactants were analytical grade and purchased from the Beijing Chemical Plant. The hydrogen and argon used possessed purity above 99.999%, while the ethylene had a purity of 99.5%. Typical experiments were performed in the horizontal quartz tube, 35 mm in diameter and 1200 mm in length, placed in a two-stage furnace. The catalyst precursor was evaporated at the first stage and delivered into the second stage by the carrier gas. The CNT arrays grew at the second stage of the furnace. The lengths of the two heat zones were 300 and 600 mm, respectively. Ferrocene was used as the catalyst precursor and ethylene was taken as the carbon source. A quartz plate was used as the CNT array growth substrate. The quartz plates were rinsed with ethanol for 10 min at first and then put in the second stage of the tube. The ferrocene was laid in a ceramic boat for controllable evaporation at a certain temperature, in the first stage of furnace. The second stage was heated to the growth temperature in the atmosphere of 95% Ar and 5% H_2 with a flow rate of the carrier gas at 600 sccm. Then the ethylene was introduced into the reactor, with a flow rate of 100 sccm. After growth for half an hour, the furnace heater was turned off and the ethylene inlet was terminated. The reactor was then cooled to room temperature under the protection of the carrier gas of Ar and H_2. The as-grown products were taken out of the reactor and peeled from the quartz plate for further characterization.

After the product collection, the morphologies of the products were characterized by a JSM 7401F scanning electron microscope (SEM) operated at 5.0 kV and a JEM 2010 transmission electron microscope (TEM) operated at 120.0 kV. The sample for TEM was prepared by sonication of about 3.0 mg of as-grown products in ethanol for 15 min and several drops were put onto a TEM copper grid. The diameter distributions of the products were obtained statistically of 200 tubes from the images recorded by SEM or TEM.

3 Results and discussion

In the floating catalyst CVD process, the ferrocene was sublimed at the first stage and decomposed into iron atoms at 470°C. The iron atoms agglomerated to form the nanoparticles for CNT growth. Kuwana and Saito predicted the formation process and the growth rate of iron nanoparticles from ferrocene [31]. Various factors, including the amount for collision, the residence time, and the collision frequency, affected the size of the iron nanoparticles. With the ferrocene concentration fixed at 280 ppm in the high temperature regime ($T = \sim$3000 K), the monodisperse model, with a constant collision frequency function, was found to be a good approximation of the particle diameter. The iron particles were about 80 nm with 10 s collision. While the temperature decreased to 1000 K, the iron catalysts were about 10 nm. When the temperature was lowered to 800 K, the size was just about 1.0 nm [31]. The numerical prediction, using the interpolative closure model, found that the iron catalyst particle can obviously be modulated by operating the parameters of ferrocene decomposition. However, in the floating catalyst for CNT array growth, the effects of the carbon formation and the substrate were complex. CNT arrays can grow in the confined domain of various parameters, including the temperature, substrate, flow rate, and gas composition. Experimental researches are important in detecting the key factors for such processes. Given that this is such a complex system, further simplifications are needed for additional experimentation. In the catalyst particle formation process, we fixed the catalyst precursor as ferrocene and the carbon source was ethylene. Since the flow effects were well understood by the computational fluid dynamic simulation and had a close relationship with the reactor size, the gas feeding rates were also fixed. In the catalyst formation process, we tested the concentration of the iron atom at the initial rate and the iron collision frequency. The iron atom concentration can be easily modulated by controlling the feeding rate of ferrocene, which dramatically affected the kinetic process of the iron catalyst formation process. The second factor of iron collision frequency can obviously be modulated by the temperature, which was CNT growth temperature in our case.

To test the effect of iron concentration, the catalyst feeding rate should be estimated first. In most researches, the ferrocene have been dissolved in the liquid carbon source, the feeding rate of ferrocene have been always kept at about 0.05–2 g/h. When gaseous carbon sources are used, the feeding rate can be controlled by the evaporated temperature. As shown in Table 1, most groups set the sublimed (or evaporated) temperature in the scale of 150–350°C. The vapor pressure of ferrocene have been a concern of many groups [32, 33]. From Emel'yanenko et al.'s recommendation [33], the correlationship of vapor pressure of the ferrocene and temperature can be expressed in (1).

$$\ln(P_e/\mathrm{Pa}) = \frac{273.6}{R} - \frac{81535.7}{R \cdot (T/\mathrm{K})} - \frac{29.6}{R} \ln\left(\frac{T/\mathrm{K}}{298.15}\right) \quad (1)$$

where P_e is the vapor pressure of ferrocene, T is the temperature, and R is the gas constant with a value of 8.3145 J/mol K. The calculated vapor pressures at corresponding, sublimed temperature, are shown in Table 1. When the sublimed temperature was higher than 150°C, the vapor pressure was higher than 4.84×10^3 Pa. The subliming rate of ferrocene can be estimated by (2) as follows:

$$\Gamma = \alpha(P_e - P_h)\sqrt{\frac{M}{2\pi RT}} \quad (2)$$

where Γ (g/s) is the feeding rate per second, α is the sublimed constant, which has a relationship to the substance composition and the contact area with a value from 0.0001 to 1. P_h is the ferrocene in the gas phase and M is the molecular weight. Table 1 shows that the flow rate and the diameter size have a similar order of magnitude, therefore, comparing the feeding rate among various studies, α was assumed to be 0.0001 for further estimation. The constant

Table 1 Feeding of catalyst precursor in floating catalyst CVD

Catalyst precursor	Evaporated temperature (°C)	Flow rate of carrier gas (sccm)	Diameter of reactor (mm)	Vapor pressure of ferrocene (Pa)[a]	Estimated feeding rate (g/s)[b]	Ref.
Ferrocene	150	~500	25	4.84×10^3	0.044	[8]
Ferrocene	200	~200	25	3.76×10^4	0.327	[16]
Ferrocene	350	~950	10	2.07×10^6	15.7	[7]
Ferrocene	60	~600	35	21.7	2.24×10^{-4}	This work
	80			93.2	9.36×10^{-4}	

[a]The vapor pressure of ferrocene was estimated by (1)

[b]The feeding rate of ferrocene was estimated by (2) with the assumption that α was 0.0001

addition of fresh gas into the reactor altered the P_h to 0 Pa. Most researches contain a feeding rate over 0.04 g/s (Table 1), which indicates that about 1.29×10^{20} iron atoms were formed in the reactor per second. Compared with the ferrocene inlet rate for the reports using liquid hydrocarbon as carbon source for CNT array growth, this was too high and the iron catalyst, with a certain size, was not sensitive to the amount of ferrocene introduction. Thus, in the present report, the first step was decreasing the evaporated temperature to 60–80°C, in which the diameter of CNTs in the array form will be modulated.

Figure 1 shows how a typical CNT array morphology grew at a low feeding rate with ferrocene sublimed at 60°C.

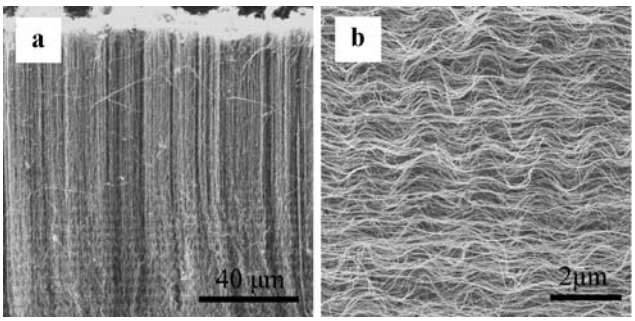

Fig. 1 (**a**) Low magnification and (**b**) high magnification of CNT arrays with ferrocene subliming at 60°C and growing at 800°C

The vertically aligned CNT arrays were peeled from the quartz substrate (Fig. 1a). With ferrocene sublimed at 60°C, and reaction temperature maintained at 800°C, the array was 200 μm in length for a 20-minute growth. No other impurities, including the amorphous carbon, iron catalyst encapsulated with carbon, could be found in the as-grown product. From the high magnification of the SEM images, there were two kinds of CNTs in the array. Some CNTs were straight, while other CNTs were curved with a tortuous factor of 1.12 ± 0.05 [34]. A similar structure was found on the CNT array grown on the plate from cyclohexane through synchronous growth with a pristine stress [34]. The CNT grows like a forest, in which the growth site is at the root of each tube, with iron catalyst particles sitting at the bottom [35]. Thus, similar CNT array synchronous growth mechanisms were discovered in the floating catalyst with ethylene as the carbon source [34]. Compared with other studies, a low catalyst feeding rate was used in the present research.

The diameter distribution of CNTs in the array can be obtained from the TEM images. Figures 2a and 2b show the CNT grown at 800°C with ferrocene sublimed at 80 and 60°C, respectively. The inserted high-resolution transmission electron microscopy (HRTEM) images indicate that as-grown CNTs contained good crystallite structure. The inner diameter of the CNTs was about 5–10 nm, while the outer diameter showed a wide distribution. For CNT arrays grown with the catalyst precursor evaporated temperature

Fig. 2 (**a**) and (**b**) TEM images, (**c**) and (**d**) diameter distribution of CNT in array form grown at 800°C with ferrocene subliming at 80 and 60°C, respectively

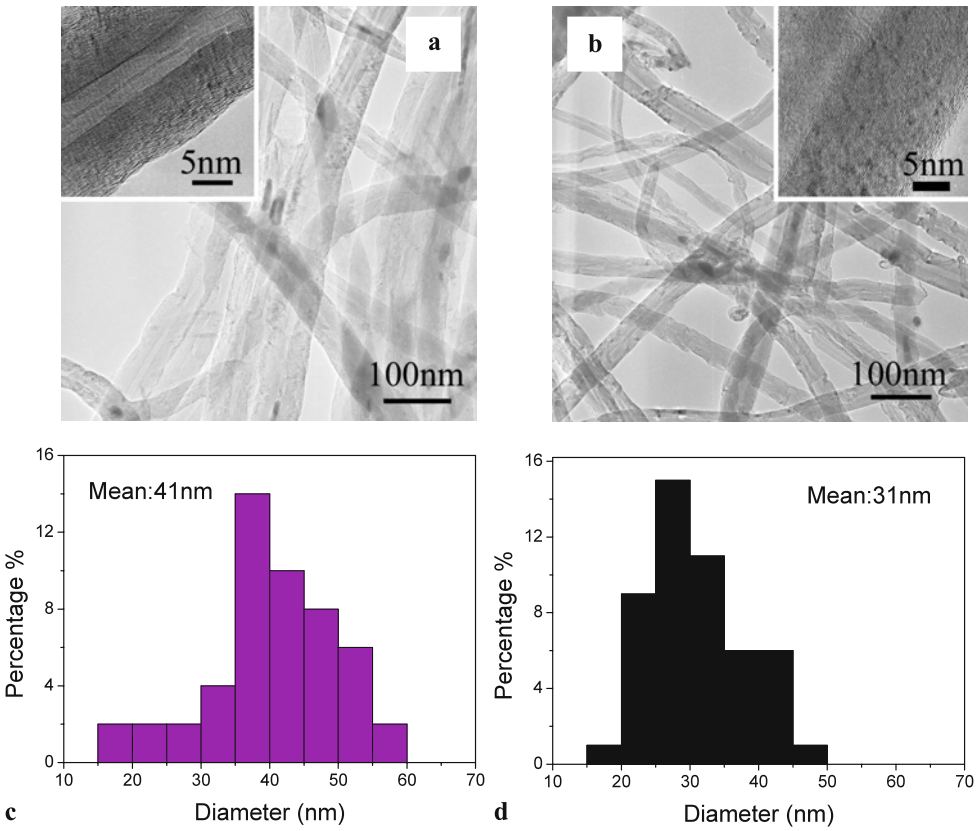

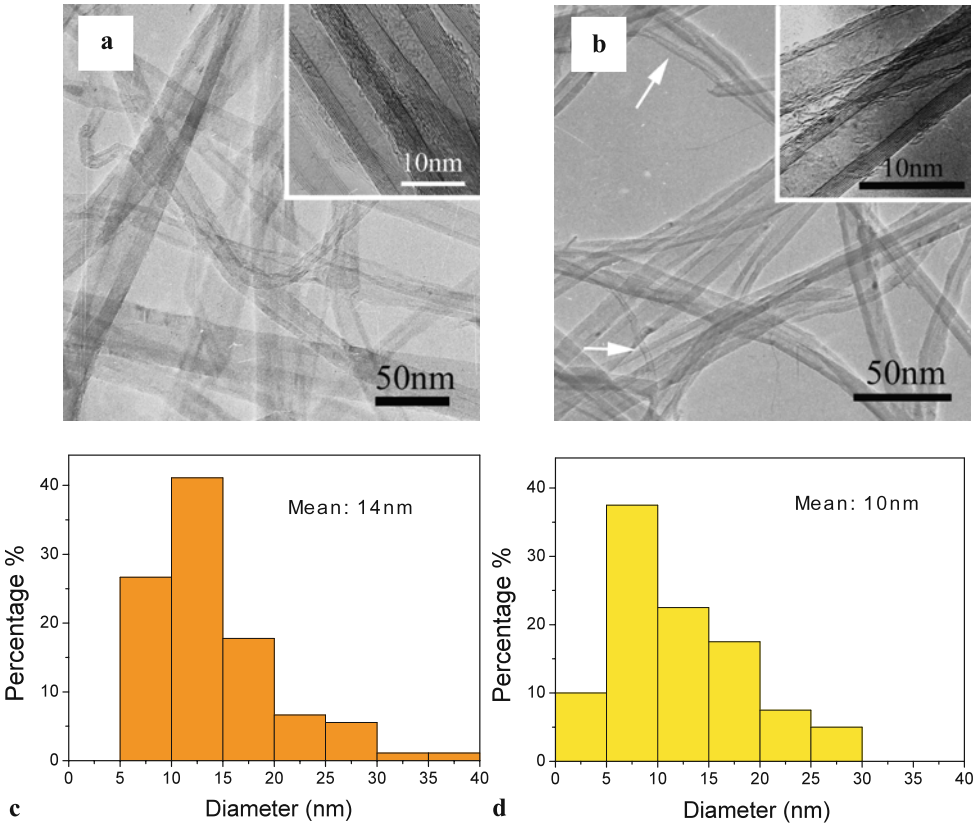

Fig. 3 (**a**) and (**b**) TEM images, (**c**) and (**d**) diameter distribution of CNT in array form grown at 700 and 600°C with ferrocene evaporation at 60°C, respectively

of 80°C, the diameter was mainly in a range of 15–80 nm (Fig. 2c), with a highest peak at 40 nm. Then mean diameter was 41 nm. For CNT arrays grown with the catalyst precursor sublimed at 60°C, no large diameter CNTs, such as 60–80 nm, could be found. The CNTs were mainly 20–60 nm, with a mean diameter of 31 nm (Fig. 2d). In the floating catalyst CVD, the ferrocene was sublimed at a low temperature in the first stage. The ferrocene vapor was transferred into the second stage furnace by carrier gas. It decomposed into iron atoms when the temperature was above 470°C. If the evaporation temperature decreased from 80 to 60°C, the amount of introduced ferrocene was diminished (as shown in Table 1). With less introduced ferrocene, less collision would occur among the iron atoms decomposed from ferrocene and the as-formed iron catalyst particles would be smaller in size. From the vapor–liquid–solid (VLS) mechanism, CNTs with smaller diameter in array form grew from the substrate [19, 20, 35]. Compared with other studies, the amount of ferrocene introduced into the reactor was much less. The smaller diameter distributions of CNTs in the array form were attributed to the sensitivity to the catalyst feeding rate.

After the catalyst formation in the gas phase, the iron nanoparticles were attached to the substrate, where further sintering took place. If the growth temperature varied, the collision frequency and sintering possibility changed, which would result in the modulation for the diameter of iron catalysts and CNTs. Here, we fixed the catalyst precursor sublimed at 60°C, and the feeding rates of the carbon source and the carrier gas were fixed as well. The TEM images of CNTs in the array form grown at 700 and 600°C are shown in Figs. 3a and 3b, respectively. HRTEM images indicated that the CNTs grown at 700°C had a diameter of about 12 nm, and the number of graphite layers was about 10. Compared with the CNTs shown in Fig. 2b, the diameters of CNTs in the array were significantly reduced. This can be further confirmed by the statistical results shown in Figs. 3c and 3d. For CNT arrays grown at 700°C, the diameters had a wide distribution of 5–40 nm with a mean diameter of 13.9 nm. The CNTs peaked at 10–15 nm. Compared with Fig. 2d, the outer diameter of the CNTs decreased dramatically. If the growth temperature had a further decrease, few-walled CNTs could be obtained, as shown in Figs. 3b and 3d. There was a wide diameter distribution of 1–30 nm with a mean diameter of 10.2 nm. The peak was at 5–10 nm. Some of the few-walled CNTs, which are indicated with the arrows in Fig. 3b, had a diameter of 3 nm. The diameter distribution was lower than the CNTs obtained from floating catalyst CVD, as reported. The sintering among small catalyst particles decreased, leading the formation of small diameter CNTs.

Meanwhile, at low temperature, the CNTs with a small diameter could be obtained, but the growth rate was slow.

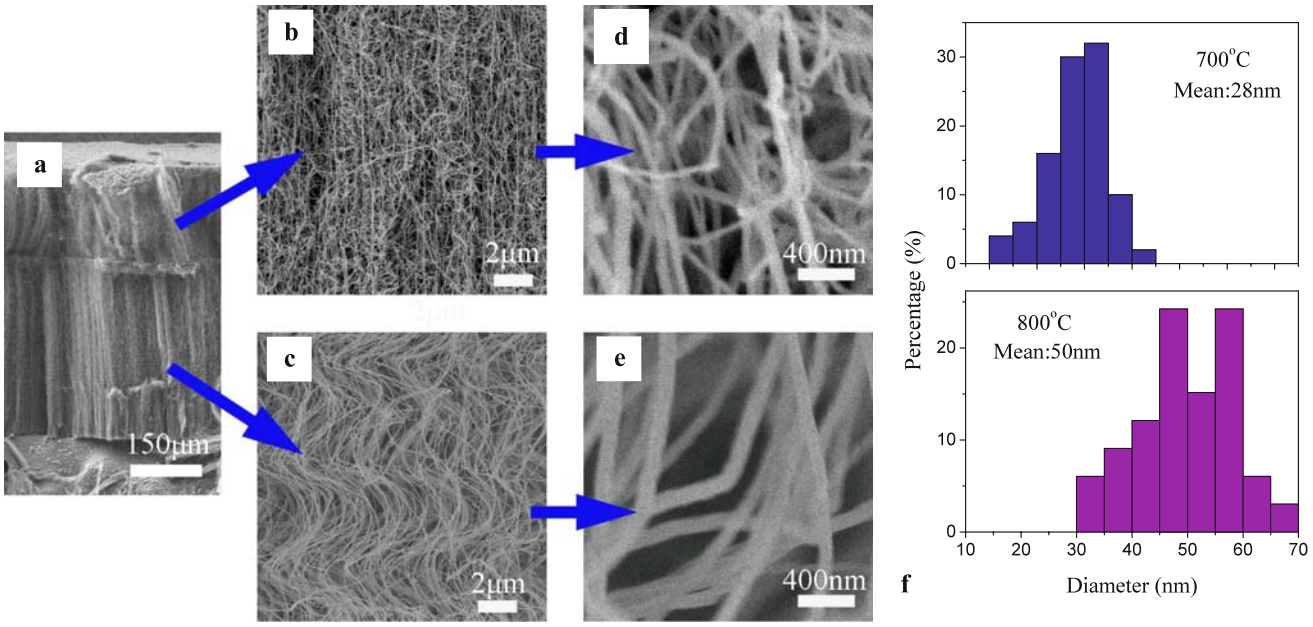

Fig. 4 (**a**) Morphology of CNT array grown at 700°C for 0.5 h and 800°C for another 0.5 h. For the root growth of CNT array in the floating catalyst CVD, the array grown at 700°C was at the top of the array. An interface was shown when the temperature increased from 700 to 800°C. (**b**), (**c**) SEM images and (**d**), (**e**) high magnification SEM images of CNT array grown at 700 and 800°C, respectively. (**f**) Diameter distribution of CNT array grown at 700 and 800°C, respectively. The diameter of CNTs grown at 700°C was smaller than those grown at 800°C

To obtain thin-walled CNTs, high temperature is needed for more effective carbon source cracking and a higher carbon atom transfer rate in the metal particles during longer CNT growth. The arrays show synchronous growth with an active growth site at the bottom of each tube. If the catalyst size can be stabilized by the carbon atoms at low temperature, for instance at 700°C, the size of the particle will be small. The carbon-coated catalyst particles activated the array growth. If the temperature were increased to 800°C, the growth rate increased. Figure 4 outlines the growth rate for the diameter of the CNTs. The array grew at 700°C for 0.5 h and at 800°C for another 0.5 h. A 10-minute heating was required for the temperature increase. The ferrocene was sublimed at 80°C. The as-grown array showed a two-layer structure. With the root growth, the short array of 200 μm corresponded with the growth at 700°C and the relatively long array of 400 μm corresponded with the growth at 800°C. This indicated a faster growth at higher temperatures. Furthermore, as shown in Fig. 4, the CNTs grown at 700°C had smaller diameters, with a mean of 28 nm. The CNTs grown at 800°C had a larger diameter, with a mean of 50 nm. The diameter of the CNTs increased with the growth temperature for an array. During CNT growth, the catalyst precursor was continuously fed into the reactor, and the iron catalyst was encapsulated and substituted [35]. At 700°C, the catalyst particles were small in size. When the temperature increased, the sintering of the catalyst particles on the substrate increased. When the catalyst was feeding continuously and the catalyst at the root was updated gradually [35], large-size catalyst particle formed at high temperatures. Thus, large-diameter CNTs were obtained. The present results indicate that the fast growth of thin-walled CNTs is still an unsolved problem in floating catalyst CVD. Furthermore, the diameter of CNT growth at 800°C or above is larger than that grown on the substrate directly. There was catalyst substitution in the floating CVD process, and the iron catalysts that easily sintered to large particle with pre-growth CNT at 700°C was distributed on the substrates.

Besides, other kinds of carbon sources, like propylene, were also used for CNT array growth. The morphologies of the as-grown products are shown in Fig. 5. In Figs. 5a and 5b, the growth temperature was fixed at 800°C, and the ferrocene evaporated temperature was 60 and 80°C, respectively. The mean diameter of the CNTs increased from 19 to 41 nm. Similarly, as the growth temperature decreased, the diameter also decreased. The diameter of CNTs, obtained from propylene showed similar trends to those obtained from the ethylene (Table 2). All of these indicate that the above-mentioned mechanisms are still effective for using propylene as carbon source. The feeding rate of the catalyst precursor and growth temperature can be changed to modulate the size of the catalyst particle, and the mean diameter of the CNT in the array form is also controllable. The diameter of the CNT can be easily modulated by the parameter of the operation using the same substrate and catalyst precursor, without other equipment or previous treatment.

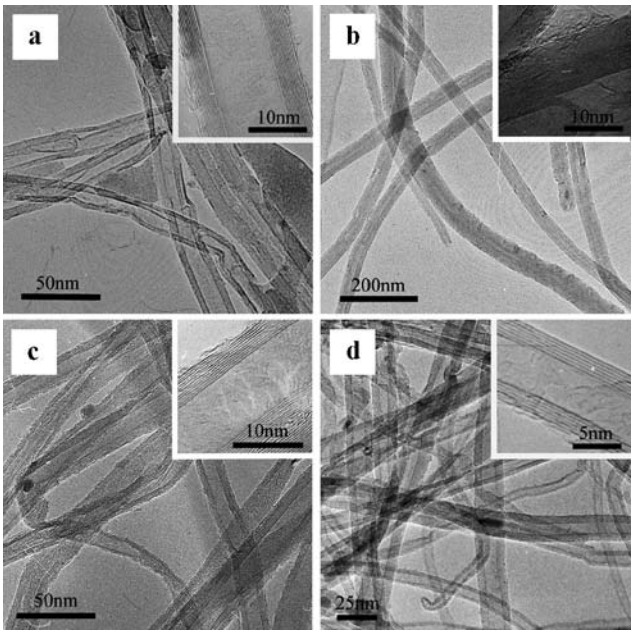

Fig. 5 TEM images of as-grown CNT array from propylene with different growth parameters. (**a**) The catalyst precursor was evaporated at 60°C, and the CNT array was grown at 800°C; in (**b**), (**c**), and (**d**), the catalyst precursor was evaporated at 80°C, and the CNT array was grown at 800, 700, and 600°C, respectively

Table 2 The mean diameter of CNTs obtained via floating catalyst CVD with ethylene or propylene as carbon sources

Carbon source	Ferrocene evaporated temperature (°C)	Growth temperature (°C)		
		600	700	800
Ethylene	60	–	–	∼31
	80	∼10	∼14	∼41
Propylene	60	–	–	∼20
	80	∼11	∼19	∼41

However, the diameter distributions, obtained from various cases, are still broad. Dedicated operation or new thoughts to modulate the size of catalyst particles and growth processes are still needed for high quality of CNT array growth.

4 Conclusions

Based on the analysis of catalyst particle formation process in floating catalyst chemical vapor deposition (CVD) instead of traditional liquid solution introduction of the carbon source and catalyst precursor ethylene was used as carbon source and together with ferrocene were sublimed into the reactor directly. The low feeding rate of catalyst precursor was taken. When the amount of ferrocene introduced into the reactor decreased, the collision decreased and small catalyst particles were formed. The mean diameter of the carbon nanotube (CNT) array, grown at 800°C, decreased from 41 to 31 nm with ferrocene sublimed temperature changing from 80 to 60°C. If the growth temperature decreased, both the sintering of catalyst particles on the substrate and the collision frequency decreased. Subsequently, the catalyst particle size further decreased. When the growth temperature was 600°C, the as-grown CNTs in the array had a wide distribution of 1–30 nm with a mean diameter of 10.2 nm, smaller than other reports by floating catalyst CVD. Given that the catalyst at the root of CNTs was gradually substituted, the catalyst cannot be stable for a long time. Thus, the diameter of CNT in the array increased with higher growth temperature. Moreover, if propylene was used as the carbon source, similar trends for the diameter change were shown. Those results provide the possibility for delicate controllable synthesis of CNT array via floating catalyst CVD.

Acknowledgements The work was supported by the Foundation for the Author of National Excellent Doctoral Dissertation of China (No. 200548), Natural Scientific Foundation of China (No. 20606020), China National Program (No. 2006CB0N0702), and Key Project of the Chinese Ministry of Education (No. 106011).

References

1. W.Z. Li, S.S. Xie, L.X. Qian, B.H. Chang, B.S. Zou, W.Y. Zhou, R.A. Zhao, G. Wang, Science **274**, 1701 (1996)
2. A.V. Melechko, V.I. Merkulov, T.E. McKnight, M.A. Guillorn, K.L. Klein, D.H. Lowndes, M.L. Simpson, J. Appl. Phys. **97**, 39 (2005)
3. Z.F. Ren, Z.P. Huang, J.W. Xu, J.H. Wang, P. Bush, M.P. Siegal, P.N. Provencio, Science **282**, 1105 (1998)
4. S.S. Fan, M.G. Chapline, N.R. Franklin, T.W. Tombler, A.M. Cassell, H.J. Dai, Science **283**, 512 (1999)
5. Y. Murakami, S. Chiashi, Y. Miyauchi, M.H. Hu, M. Ogura, T. Okubo, S. Maruyama, Chem. Phys. Lett. **385**, 298 (2004)
6. R. Andrews, D. Jacques, A.M. Rao, F. Derbyshire, D. Qian, X. Fan, E.C. Dickey, J. Chen, Chem. Phys. Lett. **303**, 467 (1999)
7. B.C. Satishkumar, A. Govindaraj, C.N.R. Rao, Chem. Phys. Lett. **307**, 158 (1999)
8. Y.T. Lee, N.S. Kim, J. Park, J.B. Han, Y.S. Choi, H. Ryu, H.J. Lee, Chem. Phys. Lett. **372**, 853 (2003)
9. X.F. Zhang, A.Y. Cao, B.Q. Wei, Y.H. Li, J.Q. Wei, C.L. Xu, D.H. Wu, Chem. Phys. Lett. **362**, 285 (2002)
10. L. Tapaszto, K. Kertesz, Z. Vertesy, Z.E. Horvath, A.A. Koos, Z. Osvath, Z. Sarkozi, A. Darabont, L.P. Biro, Carbon **43**, 970 (2005)
11. A. Barreiro, D. Selbmann, T. Pichler, K. Biedermann, T. Gemming, M.H. Rummeli, U. Schwalke, B. Buchner, Appl. Phys. A **82**, 719 (2006)
12. J.Q. Huang, Q. Zhang, F. Wei, W.Z. Qian, D.Z. Wang, L. Hu, Carbon **46**, 291 (2008)
13. C. Singh, M.S. Shaffer, A.H. Windle, Carbon **41**, 359 (2003)
14. J. Su, Y. Yu, R.C. Che, Appl. Phys. A **90**, 135 (2008)
15. R. Kamalakaran, M. Terrones, T. Seeger, P. Kohler-Redlich, M. Ruhle, Y.A. Kim, T. Hayashi, M. Endo, Appl. Phys. Lett. **77**, 3385 (2000)
16. K.E. Kim, K.J. Kim, W.S. Jung, S.Y. Bae, J. Park, J. Choi, J. Choo, Chem. Phys. Lett. **401**, 459 (2005)
17. M. Mayne, N. Grobert, M. Terrones, R. Kamalakaran, M. Ruhle, H.W. Kroto, D.R.M. Walton, Chem. Phys. Lett. **338**, 101 (2001)

18. B.Q. Wei, R. Vajtai, Y. Jung, J. Ward, R. Zhang, G. Ramanath, P.M. Ajayan, Nature **416**, 495 (2002)
19. R.T.K. Baker, P.S. Harris, R.B. Thomas, R.J. Waite, J. Catal. **30**, 86 (1973)
20. R.T.K. Baker, Carbon **27**, 315 (1989)
21. M.P. Siegal, D.L. Overmyer, P.P. Provencio, Appl. Phys. Lett. **80**, 2171 (2002)
22. F. Wei, Q. Zhang, W.Z. Qian, H. Yu, Y. Wang, G.H. Luo, G.H. Xu, D.Z. Wang, Powder Technol. **183**, 10 (2008)
23. M.J. Bronikowski, Carbon **44**, 2822 (2006)
24. K. Liu, Y.H. Sun, L. Chen, C. Feng, X.F. Feng, K.L. Jiang, Y.G. Zhao, S.S. Fan, Nano Lett. **8**, 700 (2008)
25. A.J. Hart, A.H. Slocum, J. Phys. Chem. B **110**, 8250 (2006)
26. K. Hata, D.N. Futaba, K. Mizuno, T. Namai, M. Yumura, S. Iijima, Science **306**, 1362 (2004)
27. E. Einarsson, Y. Murakami, M. Kadowaki, S. Maruyama, Carbon **46**, 923 (2008)
28. W.H. Wang, T.H. Hong, C.T. Kuo, Carbon **45**, 97 (2007)
29. R. Xiang, G. Luo, W. Qian, Y. Wang, F. Wei, Q. Li, Chem. Vap. Depos. **13**, 533 (2007)
30. A.Y. Cao, X.F. Zhang, C.L. Xu, J. Liang, D.H. Wu, X.H. Chen, B.Q. Wei, P.M. Ajayan, Appl. Phys. Lett. **79**, 1252 (2001)
31. K. Kuwana, K. Saito, in *Proceedings of the Combustion Institute* (Vol. 31, p. 1857) (2007)
32. M.J.S. Monte, L. Santos, M. Fulem, J.M.S. Fonseca, C.A.D. Sousa, J. Chem. Eng. Data **51**, 757 (2006)
33. V.N. Emel'yanenko, S.P. Verevkin, O.V. Krol, R.M. Varushchenko, N.V. Chelovskaya, J. Chem. Thermodyn. **39**, 594 (2007)
34. Q. Zhang, W.P. Zhou, W.Z. Qian, R. Xiang, J.Q. Huang, D.Z. Wang, F. Wei, J. Phys. Chem. C **111**, 14638 (2007)
35. R. Xiang, G.H. Luo, W.Z. Qian, Q. Zhang, Y. Wang, F. Wei, Q. Li, A.Y. Cao, Adv. Mater. **19**, 2360 (2007)